Current issue

[Comparing phosphoproteomic enrichments]

[Chromosomal-deletion engineering simplified]

[A SLIC new cloning method]

Current issue table of contents

Latest highlights

ADVANCE ONLINE PUBLICATION

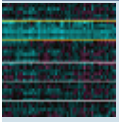

Easy but specific siRNA libraries

Article by Kittler *et al*

Enzymatic digestion of long dsRNA is an easy way to generate siRNAs for gene silencing. The efficiency and specificity of these endoribonuclease-prepared small interfering RNAs (esiRNAs) compared to well-designed siRNAs has been questioned. Buchholz and colleagues describe improved esiRNA libraries that should alleviate these concerns.

ANNOUNCEMENT

Commenting forum for *Nature Methods* FREE!

Methagora

Add your comments or propose a discussion topic for our online forum. Click the *methagora* link above to see why we think this is important.

Also on *methagora*: a new strategy to reduce photobleaching in single- and multiphoton microscopy. What controls for RNAi screens? Do GPCRs form functional dimers? Have your say!

ADVANCE ONLINE PUBLICATION

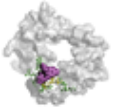

Labeling amyloid

Article by Roberti *et al.*

Fluorescence-based methods to study amyloid plaque formation have been hindered by the tendency of fluorescent tags to affect protein aggregation. Jovin and colleagues show that biarsenical labeling of α-synuclein does not appear to alter the protein's function and can be used to study the dynamics of amyloid deposit formation in living cells.

ADVANCE ONLINE PUBLICATION

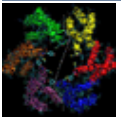

Crossing the gap

Article by Hernandez *et al.*

Gap junction-mediated transfer of intracellular second messengers is an important route of intercellular communication but is generally assessed using exogenous markers. In contrast, Mammano and colleagues quantitatively measure the transfer of endogenous second messengers through these channels.

RESEARCH HIGHLIGHTS

APPLICATION NOTES

Unitary permeability of gap junction channels to second messengers measured by FRET microscopy

Victor H Hernandez[1,5], Mario Bortolozzi[1,5], Vanessa Pertegato[1,2], Martina Beltramello[1], Michele Giarin[3], Manuela Zaccolo[1,2], Sergio Pantano[1,4] & Fabio Mammano[1,3,4]

Gap junction channels assembled from connexin protein subunits mediate intercellular transfer of ions and metabolites. Impaired channel function is implicated in several hereditary human diseases. In particular, defective permeation of cAMP or inositol-1,4,5-trisphosphate ($InsP_3$) through connexin channels is associated with peripheral neuropathies and deafness, respectively. Here we present a method to estimate the permeability of single gap junction channels to second messengers. Using HeLa cells that overexpressed wild-type human connexin 26 (HCx26wt) as a model system, we combined measurements of junctional conductance and fluorescence resonance energy transfer (FRET) emission ratio of biosensors selective for cAMP and $InsP_3$. The unitary permeabilities to cAMP ($47 \times 10^{-3} \pm 15 \times 10^{-3}$ μm³/s) and $InsP_3$ ($60 \times 10^{-3} \pm 12 \times 10^{-3}$ μm³/s) were similar, but substantially larger than the unitary permeability to lucifer yellow (LY; $7 \pm 3 \times 10^{-3}$ μm³/s), an exogenous tracer. This method permits quantification of defects of metabolic coupling and can be used to investigate interdependence of intercellular diffusion and cross-talk between diverse signaling pathways.

In chordates, intercellular communication based on gap junctions relies on channels formed by protein subunits of the connexin family, whose members are named according to their molecular mass[1]. Connexins have highly conserved sequences with four transmembrane domains separating one cytoplasmic and two extracellular loops, with cytoplasmic carboxy- and amino-terminal ends. Each cell contributes a hexamer of connexins forming a hemichannel, or connexon, which, in the narrow extracellular cleft, interacts and aligns with another connexon from the adjacent cell. Mutations in connexin genes are implicated in various hereditary human diseases, including cardiovascular anomalies, peripheral neuropathies, deafness, skin disorders and cataracts[2].

Several endogenous ions and low-molecular-weight species cross gap junction channels, including all current-carrying anions and cations, glycolytic intermediates, vitamins, amino acids and nucleotides, as well as some of the more important second messengers involved in cell signaling, such as $InsP_3$ and cAMP[3]. $InsP_3$ (molecular mass, 414 Da; charge, –6) is the first and the principal inositol phosphate that is formed by inositol lipid hydrolysis resulting from G protein–linked receptor stimulation of phospholipase C, and it is considered a global messenger molecule[4]. $InsP_3$ molecules diffuse throughout the cell nearly unbuffered, with diffusion coefficient D in cytoplasm on the order of 280 μm²/s and a lifetime up to ~60 s (depending on cell type); when they interact with specific receptors ($InsP_3R$) present in the endoplasmic reticulum, Ca^{2+} is liberated, raising its concentration in the cytosol[5].

Like $InsP_3$, cAMP (molecular mass, 329 Da; charge, –1) is a ubiquitous intracellular second messenger that affects cell physiology by directly interacting with effector molecules, including cAMP-dependent protein kinases (PKA), cyclic nucleotide-gated ion channels (CNG channels), hyperpolarization-activated channels[6] and the guanine exchange factor EPAC[7]. cAMP is generated exclusively at the plasma membrane, but its degradation can occur throughout the cytoplasm, where its lifetime is ~60 s. The D of cAMP has been estimated at 780 μm²/s in Aplysia sensory neurons[8], although this value is probably too high, as the D of Ca^{2+} (40 Da) is 790 μm²/s in water.

The intercellular transfer of ions and endogenous solutes through gap junction channels serves a variety of specific functions. The procedures that have gained wide acceptance in assaying the molecular permeability of connexins, however, are dependent on the introduction into living cells of exogenous markers, which are then traced in their individual intercellular movements[3]. In an 'exotic' assay, the local UV uncaging of NPE-HCCC2 generates fluorescent HCCC2 in one cell to visualize dye transfer to neighboring coupled cells[9]. A more commonly used dye is LY (molecular weight, 443 Da; charge, –2), whose high fluorescence efficiency ensures its detection at minute levels. Studies based on LY and other charged tracers, such as the Alexa series of fluorescent probes, show clearly that the permeability profile of each connexin channel is distinct[3]. As even modest selectivity at cellular junctions could have a great effect on the strength, character and location of the transmitted signal, the mechanisms of such discrimination are of acute biological and medical interest[10]. For

[1]Istituto Veneto di Medicina Molecolare and [2]Istituto Dulbecco Telethon, Fondazione per la Ricerca Biomedica Avanzata, 35129 Padova, Italy. [3]Dipartimento di Fisica 'G. Galilei' dell'Università di Padova and [4]Consorzio Nazionale Interuniversitario per le Scienze Fisiche della Materia, 35131 Padova, Italy. [5]These authors contributed equally to this work. Correspondence should be addressed to F.M. (fabio.mammano@unipd.it).

RECEIVED 2 JANUARY; ACCEPTED 22 FEBRUARY; PUBLISHED ONLINE 11 MARCH 2007; DOI:10.1038/NMETH1031

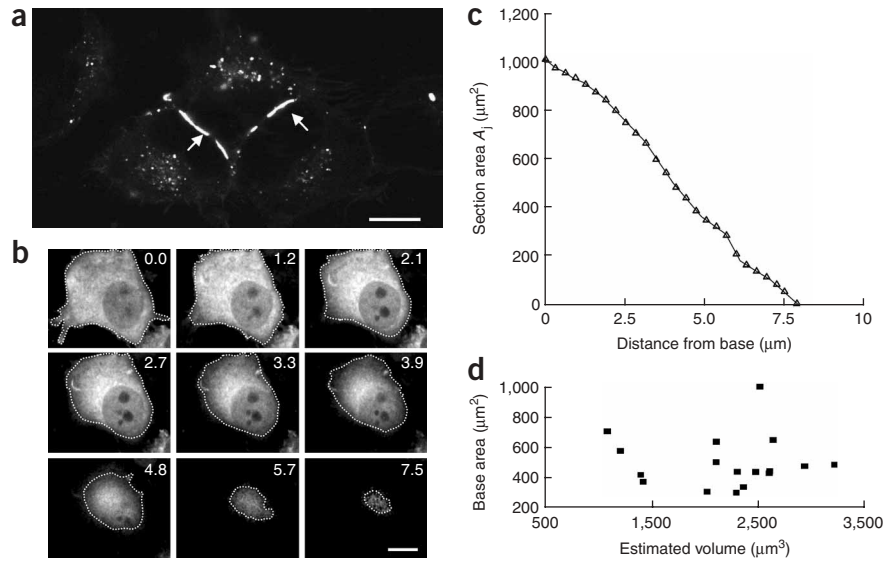

Figure 1 | HeLa cell transfection and cell volume estimate. (**a**) Confocal fluorescence image of three HeLa cells transfected with EYFP-HCx26wt; note junctional plaques (arrows) and fluorescence puncta scattered in the cytoplasm. Scale bar, 10 μm. (**b**) Through-focus optical sections, taken at 0.3-μm intervals, of HeLa cells cotransfected with HCx26wt and the cAMP biosensor H30; numbers on each frame are distance from cell base in μm. Scale bars, 10 μm. (**c**) Cell area section derived from the analysis of the through-focus sequence in **b**, plotted against distance from cell base. (**d**) Scatterplot of cell base area against estimated cell volume for $n = 17$ cells in this study.

instance, defective permeation of cAMP through gap junctions between adjacent cytoplasmic loops of myelinating Schwann cells is thought to underlie certain forms of X-linked Charcot-Marie-Tooth disease[11]. However, extrapolations from dye permeation studies present major difficulties because of the different shapes, flexibilities, charges and charge distributions of these molecules[10]. Thus, how exactly these measurements relate to the selective permeability of endogenous solutes remains obscure.

Measurement of endogenous messengers' transit has been so far problematic mostly owing to lack of direct reporters. For example, to compare the transfer rate of cAMP through gap junction channels formed by different connexins, CFTR-mediated chloride currents[12], Ca^{2+} currents through CNG channels and Ca^{2+} imaging[13] are used as sensors for cAMP. The transfer of $InsP_3$ also is usually detected indirectly[14]. Using Ca^{2+} imaging as the readout for $InsP_3$ dynamics, we recently demonstrated that $InsP_3$ permeability is altered in a deafness mutant of Cx26 (ref. 15).

Here, in an effort to develop direct, quantitative and reproducible means to monitor the flux of cAMP or $InsP_3$ through recombinant gap junction channels, we used novel ratiometric fluorescent biosensors that exploit the phenomenon of FRET for the quantitative monitoring of second-messenger concentrations in single living cells in real time[16,17]. Measurement of junctional conductance, g_j, by the dual whole-cell patch-clamp technique, combined with knowledge of the unitary conductance, γ, of homotypic channels formed by HCx26wt, allowed estimation of the number of active gap junction channels, allowing the determination of the unitary—that is, single-pore—permeability coefficient, p_u, for $InsP_3$ and cAMP. The flux of LY was quantified similarly, for comparison. This approach may have general applicability, as it provides fast and reliable estimates of connexin channel permeability to second messengers and permits the study of their role in the physiology and pathology of cell-cell communication. The method can readily be combined with multispectral imaging of other fluorescent reporters to investigate cross-talk among signaling pathways[18].

RESULTS

Permeability assay development

We performed experiments at room temperature (21–23 °C), following protocols described in the Methods (also see **Supplementary Methods** online). Briefly, we estimated gap junction permeability in HeLa cells transfected with HCx26wt (**Fig. 1a**). All compounds of interest were delivered intracellularly by passive diffusion out of patch pipettes under whole-cell recording conditions. We monitored molecular transfer between cell pairs coupled by homomeric HCx26wt channels with a wide-field fluorescence microscope, directly measuring cell volume, V, by digital optical sectioning[18] (**Fig. 1b–d**). Unless otherwise stated, results are expressed as mean ± s.e.m. and n is the number of transfected cell pairs studied.

Unitary permeability to LY

The estimate of unitary permeability p_u (see **Supplementary Methods**) requires measurement of the junctional transfer rate across the plaque (**Fig. 2**):

$$k_j = \frac{dc_2/dt}{c_1 - c_2}$$

(with units of s^{-1}). In the expression above, c_1 and c_2 indicate intracellular concentrations in cell 1 and cell 2 after delivery of LY to cell 1 (WC_1; see **Fig. 2a**). Concentration has been shown to be directly related to LY fluorescence emission intensity, spatially integrated and divided by V (ref. 19), over a range of ~0–2 mM (ref. 20). This range easily accommodates the values reached in cell 1 and cell 2 as a result of the pipette concentration of 440 μM used for the LY experiments. Therefore, we drew separate regions of interest (ROIs) on the fluorescence images along the contours of each cell at its base, then computed c_1 and c_2 by summing the background-subtracted intensity (gray) levels, F, of all image pixels within each ROI and dividing the result by the volume of the corresponding cell:

$$c_{1,2} \equiv \left(\sum F\right)_{1,2} \Big/ V_{1,2}$$

(with units of gray level per μm^3), where the subscript 1,2 denotes that there are two equations of this form, one for c_1 and one for c_2. After a suitable delay, the whole-cell configuration was achieved in the coupled cell as well (WC_2; **Fig. 2a**), which permitted the measurement of junctional conductance:

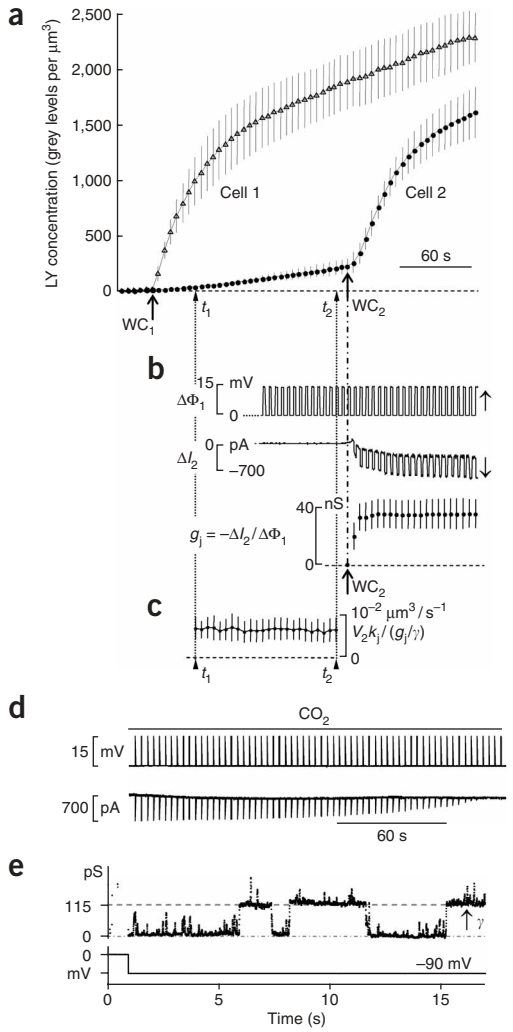

Figure 2 | Estimate of HCx26wt permeability to LY in pairs of transfected HeLa cells. (**a**) Average fluorescence traces ($n = 3$) obtained by illuminating the field at $\lambda_{ex} = 425$ nm to observe LY spread (emission wavelength $\lambda_{em} = 540$ nm). LY (0.44 mM) was delivered to cell 1 under whole-cell recording conditions (WC_1). Ordinates are LY concentration. (**b**) Top trace, voltage steps, $\Delta\Phi_1$, applied to cell 1; middle trace, current changes, ΔI_2, evoked in cell 2 while holding it at a constant potential to measure junctional current $I_j = -\Delta I_2$; bottom trace, average intercellular conductance $g_j = -\Delta I_2/\Delta\Phi_1$ measured after achieving the whole-cell configuration in cell 2 (WC_2). (**c**) Estimated unitary permeability to LY. (**d**) Blockade of junctional current by CO_2. (**e**) Conductance changes (top trace) owing to gating of a single channel, formed by HCx26wt, after application of a transjunctional potential difference $\Phi_j = -90$ mV (bottom trace); estimated unitary conductance $\gamma = 115$ pS (arrow).

$$g_j = -\Delta I_2/\Delta\Phi_1$$

by dual whole-cell current recording (see Methods). Here, ΔI_2 is change in current elicited in cell 2 owing a voltage step $\Delta\Phi_1$ in cell 1 (**Fig. 2b**). In separate control experiments, g_j was stable for time intervals that exceeded the duration of these measurements. Thus, the microscopic parameter p_u (with units of µm³/s), which quantifies the diffusive flow through a single channel, was computed as

$$p_u = V_2 k_j/(g_j/\gamma)$$

(see **Supplementary Methods**), where $\gamma = 115$ pS is unitary conductance of HCx26wt channels (**Fig. 2e**). In the expression above, g_j/γ serves as an estimate for N_{pore}, the number of open gap junction channels in the plaque (see Methods). The unitary permeability p_u estimated from the above formula was constant for the greatest part (interval t_1–t_2) of the interval between the WC_1 and WC_2 events ($\sim$2 min), indicating that the method is internally consistent (**Fig. 2c**). In separate control experiments, LY fluorescence in cell 1 reached a steady state within 10 min of the WC_1 event (data not shown).

We routinely applied CO_2 (**Fig. 2d**) to prove that solute transfer occurred through gap junction channels and that cytoplasmic bridges were not responsible for the observed fluorescence changes in the coupled cell[20]. Throughout this study, we retained for analysis only data sets where complete electrical uncoupling by CO_2 was demonstrated at the end of data acquisition. For LY, this procedure yielded an average $p_u = (7 \pm 3) \times 10^{-3}$ µm³/s ($n = 3$).

It could be argued that binding to cytoplasmic and/or nuclear elements[21] might contribute to underestimation of permeability to LY. Indeed, if tracer binding is appreciable and approximately the same in both cells, the time course of this process is indistinguishable from free diffusion with a slower junctional transfer rate. However, our control experiments, performed with a two-photon microscope (see **Supplementary Methods**), confine excess LY fluorescence to no more than 10% (8 ± 1%, $n = 3$; data not shown). This is a consequence of binding (prevalently) nuclear structures; excluding the nucleus from the cell volume in the computation of the p_u for LY yielded a result that overlapped, within the experimental error, that reported above.

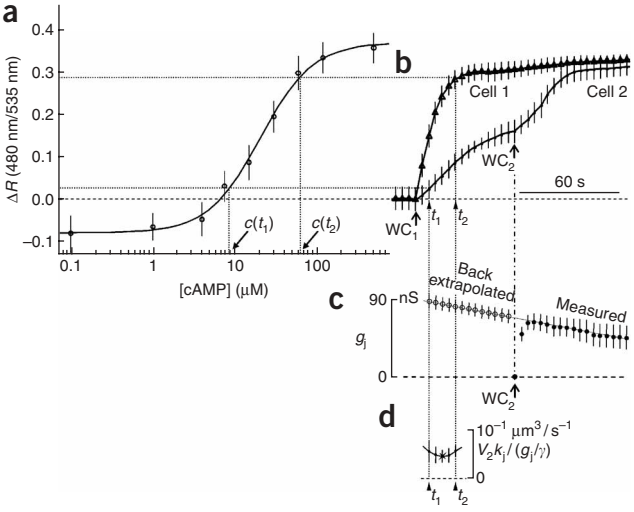

Figure 3 | Estimate of HCx26wt permeability to cAMP in pairs of transfected HeLa cells. (**a**) Concentration-response curve for the cAMP biosensor H30 ($n \geq 5$ cells at each concentration). Ordinates are background-subtracted FRET emission ratio changes ΔR measured from prestimulus ratio R_0. (**b**) Average FRET ratio traces ($n = 5$) obtained by delivery of 120 µM cAMP to cell 1 under whole-cell recording conditions (WC_1), followed by delivery to cell 2 (WC_2). (**c**) Intercellular conductance g_j measured after achieving the whole-cell configuration in cell 2 (filled symbols) and back-extrapolated to the WC_1–WC_2 interval (open symbols). (**d**) Estimated unitary permeability to cAMP.

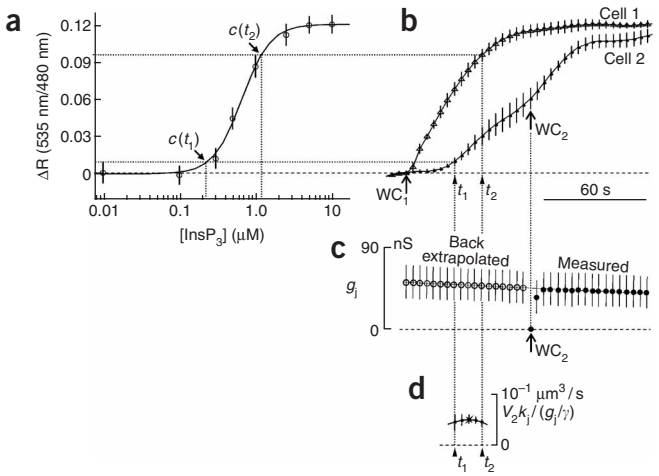

Figure 4 | Estimate of HCx26wt permeability to $InsP_3$ in pairs of transfected HeLa cells. (**a**) Concentration-response curve for the $InsP_3$ biosensor, LIBRA ($n \geq 5$ cells at each concentration). Ordinates are background-subtracted FRET emission ratio changes ΔR measured from prestimulus ratio R_0. (**b**) Average FRET ratio traces ($n = 4$) obtained by delivery of 5 μM $InsP_3$ to cell 1 under whole-cell recording conditions (WC_1), followed by delivery to cell 2 (WC_2). (**c**) Intercellular conductance g_j measured after achieving the whole-cell configuration in cell 2 (filled symbols) and back-extrapolated to the WC_1–WC_2 interval (open symbols). (**d**) Estimated unitary permeability to $InsP_3$.

Fluorescence resonance energy transfer assay

The approach highlighted above can be adapted, in principle, to any solute whose concentration change can be traced back to a fluorescence measurement. To monitor optically the transfer of cAMP (**Fig. 3**), we cotransfected HeLa cells with HCx26wt and a selective ratiometric FRET biosensor, here named H30 (ref. 16). To construct the H30 dose-response curve for cAMP, we patch-clamped transfected cells with various concentrations of cAMP in the pipette. We used ratiometric FRET microscopy (**Supplementary Methods**) to measure the steady-state levels of the background-subtracted FRET ratio signals, which were averaged and plotted against the corresponding pipette concentration. The EC_{50} for cAMP in these cells, 20 μM, is close to the previously reported value[16]. The results (**Fig. 3a**) also indicate that the FRET emission ratio of the H30 biosensor accurately traced cAMP concentration in the range from ~8 μM to ~60 μM. To monitor cAMP transfer through HCx26wt channels, we patch-clamped HeLa cell pairs with pipettes containing 120 μM of this messenger. To quantify p_u, we estimated the junctional transfer rate k_j as

$$k_j \cong \frac{dR_2/dt}{R_1 - R_2}$$

within a subinterval (t_1–t_2) during which the ratiometric FRET signals $R_{1,2}$ evoked by delivery of cAMP to cell 1 (WC_1; **Fig. 3b**) were approximately proportional to the corresponding cAMP concentrations $c_{1,2}$. We then delivered the same intracellular solution to cell 2 (WC_2; **Fig. 3b**) through a second patch-clamp pipette, with the double purpose of appraising the sensitivity of cell 2 to cAMP and measuring the junctional conductance g_j (**Fig. 3c**).

We similarly assayed diffusion of $InsP_3$ through HCx26wt channels using a recently described FRET-based molecular biosensor named LIBRA[17] (**Fig. 4**), which showed submicromolar sensitivity to $InsP_3$, with EC_{50} of 0.64 μM. This estimate agrees with the previously reported EC_{50} value[17] and is consistent with the sensitivity of the $InsP_3$-binding domain of rat type 3 $InsP_3$ receptor[22]. According to the LIBRA dose-response curve to $InsP_3$ (**Fig. 4a**), the FRET emission ratio accurately traced $InsP_3$ concentration in the range from ~0.2 μM to ~1.2 μM. To monitor second-messenger transfer through HCx26wt channels, we delivered $InsP_3$ from patch pipettes at a concentration of 5 μM (**Fig. 4b**).

In these and other preliminary experiments, in which dual patch-clamp recording conditions were maintained for >3 min, g_j tended to decline over time (**Fig. 3c** and **Fig. 4c**). Progressive closure of gap junction channels (chemical gating[23]) is not surprising and can be ascribed to metabolic state alterations resulting from the intracellular solutions used in these experiments (see Methods). Therefore, in each cell pair stimulated with cAMP or $InsP_3$, the values of g_j were back-extrapolated and, for internal consistency, p_u was estimated from the stationary values of $V_2\, k_j / (g_j/\gamma)$ within the t_1–t_2 interval (starred points in **Fig. 3d** and **Fig. 4d**). Results for LY, cAMP and $InsP_3$ are summarized in **Table 1**.

DISCUSSION

Differences in LY permeability among different connexins have been amply documented, yet the analysis is complicated by the fact that selectivity of gap junction channels formed by different connexins does not correlate with channel conductance[3,10]. Indeed, LY has great difficulties traversing channels formed by HCx30wt, despite the main state unitary conductance of the latter ($\gamma = 160$ pS) being larger than the γ of the closely related HCx26wt[15]. The first quantitative study of LY transfer in HeLa transfectants expressing Cx43 channels (main unitary conductance $\gamma = 55$ pS) set p_u at 1.246×10^{-3} μm³/s, corresponding to the flux across a single channel, $J_{pore} = p_u(c_1 - c_2)$, of 0.75 molecule per channel per second, driven by a concentration difference $c_1 - c_2 = 1$ μM; consequently, the dye was placed in the category of relatively impermeable[20]. More recent assays have reported p_u values scattered in a wide range, from 1.28×10^{-3} μm³/s to 34×10^{-3} μm³/s (ref. 19). The reason for the data spread is unclear, but (yet unknown) regulatory mechanisms have been proposed to affect affinities and/or partitioning of permeant molecules into the pore. However, the published mean permeability of Cx43 to LY, $p_u = 6.2 \times 10^{-3}$ μm³/s (ref. 19), is close to our estimate for the HCx26wt channel (**Table 1**), which predicts the transit of 4.2 dye molecules per channel per second for $c_1 - c_2 = 1$ μM.

Table 1 | Properties of LY, cAMP and $InsP_3$ related to permeation through HCx26wt pores

	LY	cAMP	$InsP_3$
Formula	$C_{13}H_9N_5O_9S_2$	$C_{10}H_{12}N_5O_6P$	$C_6H_9O_{15}P_3$
Charge	−2	−1	−6
Molecular mass (Da)	443	329	414
Bulk diffusion coefficient (μm²/s)	200[a]	780[b]	283[c]
Minor crystallographic diameter (Å)	8.5[d]	5.2	7.2
Volume of receiving cell, V_2 (μm³)	1,917 ± 217	1,610 ± 215	2,208 ± 280
Junctional conductance, g_j (nS)	39 ± 9	87 ± 8[e]	54 ± 18[e]
Junctional transfer rate, k_j (10^{-3} s^{-1})	1.1 ± 0.4	23 ± 12	13 ± 5
Unitary permeability, p_u (10^{-3} μm³/s)	7 ± 3[d]	47 ± 15[d]	60 ± 12[d]
n	3	5	4

[a]Reference 21. [b]Reference 8. [c]Reference 5. [d]This work. [e]Back-extrapolated, as in **Figure 3c** and **Figure 4c**.

On the basis of analysis of LY transit, it has been suggested that the selectivity properties of Cx43 channels might exclude the rapid transit of specific solutes such as cAMP and $InsP_3$ (ref. 20). In this vein, studies of mechanically induced calcium waves in rat osteosarcoma cell lines have suggested that gap junction communication mediated by either Cx43 or Cx45 does not allow enough passage of $InsP_3$ to elicit release of intracellular calcium stores in neighboring cells[10]. This conclusion has been challenged, for instance, by an analysis of Ca^{2+} wave propagation in cultures of HeLa cells transfected with Cx43, Cx32 and Cx26, which were reported to have similar permeabilities to the diffusing messenger[24].

Our results show substantially higher p_u for $InsP_3$ or cAMP than for LY in channels formed by HCx26wt (**Table 1**), with mean permeability ratios >6 for both cAMP/LY and $InsP_3$/LY. On the basis of the direct estimate of LY accumulation within the cells, we excluded binding to cytosolic and/or nuclear elements as a confounding factor in our estimate of p_u. Likewise, the LY leak across the plasma membrane in HeLa cells is less than 3% over a 15-min interval[20]; therefore, the nonjunctional permeability of LY was insignificant in our experiments.

Notably, in the presence of a point mutation in the second transmembrane helix, M2, of HCx26wt (valine to leucine at position 84, V84L), both the unitary conductance and the permeability to LY remain basically unaffected, whereas permeability to $InsP_3$ decreases greatly[15]. In fact, the permeant molecules studied here have linear dimensions close to the diameter of the channel pore, estimated from an all-atom model of the HCx26wt connexon (see **Supplementary Discussion** and **Supplementary Fig. 1** online), suggesting the possibility of specific interactions with pore-lining residues. Not withstanding the obvious coarseness of our theoretical structure, this approach has been successfully applied to the analysis of a mutant Cx26 with threonine substituted for methionine at position 34 (M34T)[25].

It is also noteworthy that, on the basis of its size and bulk diffusion coefficients alone, one would expect a lower p_u for $InsP_3$ than for cAMP, whereas the actual difference is not statistically significant (**Table 1**). However, the maximal percentage ratio change $\Delta R/R_0$ recorded with LIBRA is about fourfold smaller than that recorded with H30. Therefore, this estimate might still be considerably improved by use of a cytosolic $InsP_3$ sensor with low $InsP_3$ binding affinity and increased signal-to-noise ratio[26].

It is straightforward to extend these measurements to FRET reporters selective for cGMP[27]. In combination with multispectral imaging of Ca^{2+} fluorescent reporters, this could permit exploration of the mechanisms that regulate local and intercellular diffusion. Ca^{2+}, cAMP, cGMP and $InsP_3$ fluctuations could also be quantified in networks of coupled cells and tissues subject to different stimuli, and under conditions where the diffusion of the second messenger is manipulated or altered by genetic defects.

METHODS

Cell culture and transfection. We cultured a clone of HeLa cells that was essentially devoid of connexins (see Acknowledgments) according to standard procedures, as described[28]. We transfected cells 24 h after plating, using the Lipofectamine transfection protocol (Gibco, Invitrogen), with a previously described EYFP-HCx26wt fusion construct[28], to visualize gap junction plaques (**Fig. 1a**). We then used this construct in experiments involving intracellular delivery of LY, as well as in the measurement of unitary Cx26 conductance, γ, as described below. For intracellular delivery of $InsP_3$ and cAMP (see below), we cotransfected cells with the pcDNA3.1 expression vector carrying the coding region of (untagged) HCx26wt (see Acknowledgments) and an additional expression vector carrying either the $InsP_3$ reporter LIBRA[17] (see Acknowledgments) or the cAMP reporter CFP–Epac(dDEP-CD)–YFP[16] (here called H30 for brevity; see Acknowledgments). Experiments were done at room temperature 24 h after transfection.

Electrophysiology. We transferred HeLa cell cultures transfected with HCx26wt to an experimental chamber mounted on the stage of an upright wide-field fluorescence microscope (BX51, Olympus Optical Corporation) equipped with an infinity-corrected water-immersion objective (60×, 0.90 NA, LUMPlanFl, Olympus). We continuously superfused cells at 2 ml/min in a standard extracellular solution (ECS), which contained 150 mM NaCl, 5 mM KCl, 1 mM $MgCl_2$, 10 mM HEPES, 2 mM $CaCl_2$, 2 mM pyruvate and 5 mM glucose (pH 7.4). Patch pipettes were filled with an intracellular solution (ICS) containing 120 mM potassium aspartate, 10 mM tetraethylammonium chloride, 1 mM $MgCl_2$, 10 mM HEPES, 10 mM CsCl, 0.3 mM GTP-sodium and 3 mM ATP-potassium (adjusted to pH 7.2 with KOH), and filtered through 0.22-μm pores (Millipore). Pipette resistances were 3–5 MΩ when immersed in the bath.

To measure junctional conductance g_j, we maintained each cell of an isolated pair under whole-cell patch-clamp conditions with one of two List EPC-7 amplifiers and kept the two at the same holding potential, Φ_h. By stepping the voltage in one cell (cell 1) while keeping the potential of cell 2 at Φ_h, thus establishing a 15-mV transient transjunctional voltage $\Phi_j \equiv \Phi_1 - \Phi_2 = \Delta\Phi_1$, we measured junctional current, I_j, directly as a change in current in the unstepped cell ($I_j = -\Delta I_2$) (**Fig. 2b**).

To detect single–gap junction channel events and thus measure the unitary conductance, γ, we transiently switched the superfusion medium to ECS saturated with 100% CO_2 to produce carbonic acid (H_2CO_3). In its undissociated form, H_2CO_3 is membrane permeant and causes a rapid closure of the gap junction channels (**Fig. 2d**). We detected the current flowing through single gap junction channels owing to a Φ_j of –80 to –100 mV as discrete step-like events while the cells recovered from cytoplasm acidification during washout of the CO_2 (**Fig. 2e**).

Intracellular delivery of permeant molecules. For molecular transfer assays, we dissolved LY in ICS at a concentration of 440 μM. We added cAMP (120 μM, Sigma-Aldrich) to ICS together with IBMX (100 μM, Sigma-Aldrich), a phosphodiesterase inhibitor; dideoxyadenosine (1 μM, Calbiochem), a noncompetitive adenylate cyclase inhibitor; and thapsigargin (1 μM, Sigma-Aldrich), a blocker of the SERCA pumps. We added $InsP_3$ (5 μM, Calbiochem) to ICS together with diphosphoglyceric acid (3.5 mM, Sigma-Aldrich), a competitive inhibitor of $InsP_3$ phosphomonoesterases[29] that convert $InsP_3$ into $InsP_2$; and $InsP_3$-kinase inhibitor (20 μM, Calbiochem), a competitive inhibitor of the $InsP_3$ kinase that catalyzes the conversion of $InsP_3$ to $InsP_4$. All solutions were adjusted to pH 7.2 with KOH and filtered through 0.22-μm pores.

For $InsP_3$, we obtained recordings from cells superfused in ECS (see above) supplemented with 200 μM suramin, a

broad-spectrum P2Y receptor antagonist, to inhibit paracrine amplification of $InsP_3$ signals. We tested the efficacy of suramin in control experiments by exposing HeLa transfectants, loaded with fura-2, to ATP (50 μM). No detectable Ca^{2+} signals were evoked under these conditions. Methods used for these controls have been described previously[15].

In all permeability assays, both cells were approached by pipettes containing identical intracellular solutions and maintained in the cell-attach configuration. A few seconds after the onset of the recording, we ruptured the patch of membrane under the pipette sealed to cell 1 while leaving the seal intact (whole-cell recording conditions for cell 1, WC_1), allowing the compound of interest to fill the cell by passive diffusion from the patch pipette. To monitor access and membrane resistance and to synchronize image acquisition to electrical recordings, we used the 5-V pulse (FVAL) that signals active exposure of the charge-coupled device (CCD) camera used to observe the preparation. The FVAL signal was scaled down to 15 mV and fed to the patch-clamp amplifier connected to cell 1 (ref. 30). By the end of the recording interval, we also established whole-cell recording conditions for cell 2 (WC_2), which permitted an assay of its reaction to direct delivery of the compound (**Fig. 2a**) and measurement of g_j in response to scaled FVAL pulses (**Fig. 2b,c**). We then applied CO_2 to prove that transfer occurred through gap junction channels. Only cell pairs that showed complete uncoupling by the CO_2 (**Fig. 2d**) were retained for the analysis.

In separate control experiments, we monitored g_j for time intervals up to 3 min, corresponding to the duration of a standard permeability assay. With LY in the patch pipettes, g_j was constant over this time span; we therefore estimated the number of open channels $N_{pore} = g_j/\gamma$ in the interval between the WC_1 and WC_2 events from the average of g_j in a 1-min interval after the WC_2 event (excluding transients owing to incomplete seal openings). In contrast, similar control experiments revealed a progressive decline of g_j that was more pronounced for cAMP (average rate of loss 0.37 ± 0.04 nS/s, $n = 10$) than for $InsP_3$ (0.07 ± 0.03 nS/s, $n = 8$). Therefore, g_j values collected in a 1-min interval after the WC_2 event (excluding transients) were used to extrapolate back to the WC_1–WC_2 interval (**Fig. 3c** and **Fig. 4c**).

Additional methods. A description of the theoretical framework for the permeability assays, fluorescence imaging, measurement of cell volumes, estimation of permeant molecule concentration and estimation of transfer rate and unitary permeability is available in the **Supplementary Methods**.

Note: Supplementary information is available on the Nature Methods website.

ACKNOWLEDGMENTS

This work was funded by grants from Telethon Italy (GGP05131) and the European commission FP6 Integrated Project EuroHear (LSHG-CT-20054-512063) under the Sixth Research Frame Program of The European Union (to F.M.) and from Fondazione CARIPARO (to S.P.). M.Z. is supported by Telethon Italy (TCP00089, GGP05113), the Italian Cystic Fibrosis Research Foundation, the Fondazione Compagnia di San Paolo and the HFSPO (RGP1/2005). We thank K. Willecke (University of Bonn), R. Bruzzone (Institute Pasteur), K. Jalink (The Netherlands Cancer Institute) and A. Tanimura (Health Sciences University of Hokkaido) for the gifts of HeLa cells, HCx26wt, H30 and LIBRA, respectively, and T. Pozzan (University of Padova) for helpful discussions and constructive criticism.

COMPETING INTERESTS STATEMENT

The authors declare no competing financial interests.

Published online at http://www.nature.com/naturemethods
Reprints and permissions information is available online at http://npg.nature.com/reprintsandpermissions

1. Sosinsky, G.E. & Nicholson, B.J. Structural organization of gap junction channels. *Biochim. Biophys. Acta* **1711**, 99–125 (2005).
2. Gerido, D.A. & White, T.W. Connexin disorders of the ear, skin, and lens. *Biochim. Biophys. Acta* **1662**, 159–170 (2004).
3. Goldberg, G.S., Valiunas, V. & Brink, P.R. Selective permeability of gap junction channels. *Biochim. Biophys. Acta* **1662**, 96–101 (2004).
4. Irvine, R.F. 20 years of Ins(1,4,5)P3, and 40 years before. *Nat. Rev. Mol. Cell Biol.* **4**, 586–590 (2003).
5. Allbritton, N.L., Meyer, T. & Stryer, L. Range of messenger action of calcium ion and inositol 1,4,5-trisphosphate. *Science* **258**, 1812–1815 (1992).
6. Zaccolo, M., Filippin, L., Magalhaes, P. & Pozzan, T. Heterogeneity of second messenger levels in living cells. *Novartis Found. Symp.* **239**, 85–95, 150–159 (2001).
7. Bos, J.L. Epac: a new cAMP target and new avenues in cAMP research. *Nat. Rev. Mol. Cell Biol.* **4**, 733–738 (2003).
8. Bacskai, B.J. *et al.* Spatially resolved dynamics of cAMP and protein kinase A subunits in Aplysia sensory neurons. *Science* **260**, 222–226 (1993).
9. Dakin, K., Zhao, Y. & Li, W.H. LAMP, a new imaging assay of gap junctional communication unveils that Ca2+ influx inhibits cell coupling. *Nat. Methods* **2**, 55–62 (2005).
10. Harris, A.L. Emerging issues of connexin channels: biophysics fills the gap. *Q. Rev. Biophys.* **34**, 325–472 (2001).
11. Oh, S. *et al.* Changes in permeability caused by connexin 32 mutations underlie X-linked Charcot-Marie-Tooth disease. *Neuron* **19**, 927–938 (1997).
12. Qu, Y. & Dahl, G. Function of the voltage gate of gap junction channels: selective exclusion of molecules. *Proc. Natl. Acad. Sci. USA* **99**, 697–702 (2002).
13. Bedner, P. *et al.* Selective permeability of different connexin channels to the second messenger cyclic AMP. *J. Biol. Chem.* **281**, 6673–6681 (2006).
14. Saez, J.C., Connor, J.A., Spray, D.C. & Bennett, M.V. Hepatocyte gap junctions are permeable to the second messenger, inositol 1,4,5-trisphosphate, and to calcium ions. *Proc. Natl. Acad. Sci. USA* **86**, 2708–2712 (1989).
15. Beltramello, M., Piazza, V., Bukauskas, F.F., Pozzan, T. & Mammano, F. Impaired permeability to Ins(1,4,5)P3 in a mutant connexin underlies recessive hereditary deafness. *Nat. Cell Biol.* **7**, 63–69 (2005).
16. Ponsioen, B. *et al.* Detecting cAMP-induced Epac activation by fluorescence resonance energy transfer: Epac as a novel cAMP indicator. *EMBO Rep.* **5**, 1176–1180 (2004).
17. Tanimura, A., Nezu, A., Morita, T., Turner, R.J. & Tojyo, Y. Fluorescent biosensor for quantitative real-time measurements of inositol 1,4,5-trisphosphate in single living cells. *J. Biol. Chem.* **279**, 38095–38098 (2004).
18. Bastianello, S., Ciubotaru, C.D., Beltramello, M. & Mammano, F. in *Three-Dimensional and Multidimensional Microscopy: Image Acquisition and Processing XI* (ed. Conchello, J.-A.) Vol. 5324, 265–274 (San Jose, California, USA, 2004).
19. Eckert, R. Gap-junctional single-channel permeability for fluorescent tracers in mammalian cell cultures. *Biophys. J.* **91**, 565–579 (2006).
20. Valiunas, V., Beyer, E.C. & Brink, P.R. Cardiac gap junction channels show quantitative differences in selectivity. *Circ. Res.* **91**, 104–111 (2002).
21. Brink, P.R. & Ramanan, S.V. A model for the diffusion of fluorescent probes in the septate giant axon of earthworm: axoplasmic diffusion and junctional membrane permeability. *Biophys. J.* **48**, 299–309 (1985).
22. Patel, S., Joseph, S.K. & Thomas, A.P. Molecular properties of inositol 1,4,5-trisphosphate receptors. *Cell Calcium* **25**, 247–264 (1999).
23. Peracchia, C. Chemical gating of gap junction channels; roles of calcium, pH and calmodulin. *Biochim. Biophys. Acta* **1662**, 61–80 (2004).
24. Paemeleire, K. *et al.* Intercellular calcium waves in HeLa cells expressing GFP-labeled connexin 43, 32, or 26. *Mol. Biol. Cell* **11**, 1815–1827 (2000).
25. Bicego, M. *et al.* Pathogenetic role of the deafness-related M34T mutation of Cx26. *Hum. Mol. Genet.* **15**, 2569–2587 (2006).
26. Matsu-ura, T. *et al.* Cytosolic inositol 1,4,5-trisphosphate dynamics during intracellular calcium oscillations in living cells. *J. Cell Biol.* **173**, 755–765 (2006).
27. Nikolaev, V.O., Gambaryan, S. & Lohse, M.J. Fluorescent sensors for rapid monitoring of intracellular cGMP. *Nat. Methods* **3**, 23–25 (2006).
28. Beltramello, M. *et al.* Permeability and gating properties of human connexins 26 and 30 expressed in HeLa cells. *Biochem. Biophys. Res. Commun.* **305**, 1024–1033 (2003).
29. Downes, C.P., Mussat, M.C. & Michell, R.H. The inositol trisphosphate phosphomonoesterase of the human erythrocyte membrane. *Biochem. J.* **203**, 169–177 (1982).
30. Mammano, F. *et al.* An optical recording system based on a fast CCD sensor for biological imaging. *Cell Calcium* **25**, 115–123 (1999).

SUPPLEMENTARY METHODS

Theoretical framework for the permeability assays

Let dm denote the *net molar amount* of solute transferred during a time interval dt from cell 1 to cell 2 through a gap junction plaque, treated as a porous membrane of thickness h_m pierced by small cylindrical openings ("pores"). Conservation of mass requires that

$$\frac{dm}{dt} = N_{\text{pore}}\ J_{\text{pore}}$$

Equation 1

where N_{pore} is the number of open gap junction channels in the plaque and J_{pore} (mol/s) is the *net flux of solute* through a single pore. According to Fick's first law [1, 2], it is equal to

$$J_{\text{pore}} = -A_{\text{pore}}\ D_e\ \frac{\partial c}{\partial x}$$

Equation 2

Where A_{pore} is pore section area (μm^2), D_e is the effective diffusion coefficient ($\mu m^2/s$), c is *solute concentration* (mol/μm^3) and x (μm) is spatial coordinate along the pore axis. Assuming that

$$\frac{\partial c}{\partial x} = -\frac{c_1 - c_2}{h_m}$$

Equation 3

where c_1 is concentration in cell 1 and $c_2 < c_1$ is concentration in cell 2 (ref. 2) we can re-write Eq.2 as

$$J_{\text{pore}} = p_u\left(c_1 - c_2\right)$$

Equation 4

where the proportionality constant is the *unitary permeability*, i.e. the permeability of the single pore (in $\mu m^3/s$)

$$p_u \equiv A_{\text{pore}} D_e / h_m .$$

Equation 5

This is the critical parameter we sought to derive from the experiments by monitoring optically the time course of the fluorescence changes in the injected cell (cell 1) and recipient cell (cell 2). Due to influx through the gap junction channels, the concentration in cell 2 increases at a rate

$$\frac{dc_2}{dt} = \frac{1}{V_2}\frac{dm}{dt}$$

Equation 6

where V_2 is the volume of cell 2. By combining the above equations and solving for p_u we obtain

$$p_u = \frac{V_2}{N_{\text{pore}}}\frac{dc_2/dt}{c_1 - c_2}.$$

Equation 7

Thus the estimate of p_u based on Equation 7 requires the measurement of N_{pore}, V_2, c_1 and c_2. The methods used to perform these measurements are described hereafter.

Fluorescence imaging

To monitor optically the transfer of the injected compound from cell 1 to cell 2 we used fluorescence imaging in combination with patch clamp recordings. Image acquisition on the BX51 microscope was performed using software developed in the laboratory [3]. For LY, illumination was set at a wavelength of 425 nm by a fast switching monochromator (Polychrome IV, TILL Photonics, Martinsried, Germany) and directed onto the sample through a dichromatic mirror (440dclp, Chroma, Rockingham, VT, USA). Fluorescence emission was selected around 540 nm using a D540/40m filter (Chroma) to form fluorescence images on a scientific grade CCD camera (SensiCam, PCO Computer Optics GmbH, Kelheim, Germany). Image sequences were stored on disk and processed off-line using the Matlab 7.0 software package (The MathWorks, Inc., Natick, MA, USA), as described below.

To quantify the error due to LY binding to cytosolic and–or nuclear elements, we performed control experiments taking advantage of the intrinsic optical sectioning capabilities of our two-photon microscope (Radiance 2100, Biorad/Carl Zeiss MicroImaging GmbH, Gottingen, Germany) powered by a Tsunami pulsed laser (Spectra Physics/Newport Corporation, Irvine, CA, USA). HeLa cells were loaded through patch pipettes containing 440 µM LY in the presence of an equal concentration of the dye in the bathing solution. After equilibration of the intracellular concentration (approximately 10 min), LY fluorescence emission, excited at 835 nm in a thin optical slice (thickness < 1 µm), was compared to fluorescence from the surrounding medium in the same focal plane.

For $InsP_3$ or cAMP, Fluorescence Resonance Energy Transfer (FRET) images [4] were acquired by interposing a custom-made image-forming beamsplitter between the microscope output optical port and the CCD camera. The beamsplitter was equipped with a dichromatic mirror (515dcrx, Chroma) and emission filters (d480/40 and hq535/30, Chroma) for CFP-YFP emission separation, following CFP excitation at 430 nm. Sequences of image pairs were acquired synchronously at the two emission wavelengths and stored on disk for off-line processing.

In all fluorescence experiments, the effects of photobleaching were rendered virtually negligible by carefully selecting the most appropriate inter-frame interval while controlling illumination with a mechanical shutter triggered by the FVAL signal.

Measurement of cell volumes

Immediately after the end of each intracellular delivery experiment, a through-focus sequence of fluorescence images of the patch-clamped cell pair was acquired by stepping the objective along the optical (z) axis of the microscope with a resolution Δz of 250 nm or 300 nm. We obtained digital confocal sections by multi-neighbour deconvolution using a direct estimate of the microscope point-spread function (PSF), as described in ref.3. Cell section area A_j in the *j*-th deconvolved image was measured by identifying boundaries with the *Canny* edge detection algorithm [5] (Fig. 1b). Finally, we computed cell volume as

$$V = \Delta z \sum A_j$$

(Fig. 1c). In the population sampled in this study, cell base area A_1 = 500±176 μm^2 and volume V = 2190±594 μm^3 (mean ± standard deviation, n=17 in both cases) were not correlated (Fig. 1d).

Estimate of permeant molecule concentration

For LY, $c_{1,2}$ were estimated from the single-wavelength background-subtracted fluorescence emission intensities (F). For each pixel of the 12-bit CCD camera used in this study, F is an integer number comprised between 0 and 4095 (gray levels). Since F signals collected through a wide field fluorescence microscope, and integrated over cell volume, are proportional to the number of fluorescent molecules in each cell [6], pixel gray values were summed within ROIs drawn on the fluorescence images along the contours of each cell at its base. Division by cell volume then yielded an estimate of LY concentration in units of gray levels / μm^3 (see Results and Fig.2a).

For cAMP (or $InsP_3$) FRET images at the two emission wavelengths were divided pixel-by-pixel to generate an emission ratio at each sampled point. A well known advantage of dual-wavelength over single-wavelength imaging is that the rationing operation cancels out most or all of the possible variability due to the instrument efficiency and content of the fluorescent molecular sensor [7]. Thus the ratio of the fluorescence emission images yields a non-linear function of the cAMP (or $InsP_3$) concentration within the cell. Average ratio values for the FRET signals were obtained by encompassing the image of each cell within a ROI drawn along the contours of the cell base, and averaging pixel ratios within each ROI. To calibrate these spatially averaged ratio signals, R, known amounts of cAMP (or $InsP_3$) were delivered to single transfected HeLa cells through patch pipettes filled with the same solutions used for the permeability assays. Dose-response curves (Fig. 3a and Fig. 4a) are shown as ratio changes,

$$\Delta R = R - R_o,$$

vs. pipette concentration. Here R_o is pre-stimulus ratio, measured prior to achieving the whole-cell configuration (1.11±0.01, n = 6 LIBRA transfectants; 0.81±0.05, n = 6 H30 transfectants). The steady-state R values used for the dose-response curves were obtained by maintaining the whole-cell configuration for a time long enough to permit equilibration with the pipette content by passive diffusion. This time varied between few

minutes (at saturating concentrations) to more than 10 minutes (at the lowest concentrations). Throughout this process, cell viability was monitored electrophysiologically by verifying that access resistance, membrane resistance, cell capacitance and zero-current potential stayed within 10% of their initial values. Only cells meeting these multiple criteria were retained for the analysis. Dose-response data at each concentration are averages of $n \geq 5$ cells.

Estimate of transfer rate and unitary permeability

Knowledge of the dose-response curves permits to estimate the unitary permeability p_u by converting FRET ratios $R_{1,2}$ to the corresponding concentrations $c_{1,2}$ of Equation 7. Mathematically, this is equivalent to inverting the dose-response function, but in practice this operation is subjected to controllable errors only in a limited range near the inflection point, where approximate proportionality between c and R occurs. Thus unitary permeability was computed as

$$p_u = V_2 k_j / g_j / \gamma$$

where k_j indicates the junctional transfer rate that was estimated as

$$k_j \cong \frac{dR_2 / dt}{R_1 - R_2}.$$

Since p_u is a constant, internal consistency implies that the only data which ought to be retained for the analysis are those acquired during a sub-interval (t_1, t_2) of the recording period in which the time derivative of

$$V_2 k_j / g_j / \gamma$$

approaches zero (starred points in Fig. 3d and Fig. 4d).

References

1. Fick, A. Ueber diffusion. *Poggendorff's Annalen der Physik und Chemie* **94**, 59-86 (1855).
2. Benedek, G., Villars, FMH in Biological Physics Series, Vol. 2, STATISTICAL PHYSICS, Edn. Second edition. (ed. E. Greenbaum) 91-261 (Springer-Verlag New York, Inc., New York; 2002).
3. Bastianello, S., Ciubotaru, C.D., Beltramello, M. & Mammano, F. in Three-Dimensional and Multidimensional Microscopy: Image Acquisition and Processing XI, Vol. 5324, 265-274, San Jose, California; 2004).

4. Periasamy, A. & Day, R.N. in Green Fluorescent Proteins, Vol. 58. (ed. K.F. Sullivan) (Academic Press, San Diego; 1999).
5. Canny, J. A computational approach to edge detection. *IEEE Trans. Pattern Analysis and Machine Intelligence* **8**, 679-714 (1986).
6. Eckert, R. Gap-junctional single-channel permeability for fluorescent tracers in mammalian cell cultures. *Biophys J* **91**, 565-579 (2006).
7. Grynkiewicz, G., Poenie, M. & Tsien, R.Y. A new generation of Ca2+ indicators with greatly improved fluorescence properties. *J Biol Chem* **260**, 3440-3450 (1985).

SUPPLEMENTARY DISCUSSION

Structural models of HCx26wt and permeant molecules

To gain further insight into the permeation mechanism, we constructed an atomic model of the trans-membrane portion of the HCx26wt connexon (Supplementary Figure 1) starting from the Cα model of mouse Cx32 [1]. Molecular dynamics (MD) simulations were used to achieve structural relaxation of the model, in which the tilting of the pore-lining α helices is responsible for the narrowing of the pore at the boundary with the extracellular gap (Supplementary Figure 1, b), with a major diameter $2a \approx 17.5$ Å.

Diffusion through porous membranes can been modelled by an equation due to Renkin [2], which predicts

$$p_u = D\frac{\pi a^2}{\Delta x}\left(1-\frac{r}{a}\right)^2 \cdot \left[1-2.1\left(\frac{r}{a}\right)+2.09\left(\frac{r}{a}\right)^3-0.95\left(\frac{r}{a}\right)^5\right]$$

Here r is molecular radius, D is diffusion coefficient in the bulk (see Table 1, main text) and Δx is pore length (9 nm in our model, based on Ref. 3). The above equation has been tested experimentally for r/a values in the range from ~0.05 to ~0.32 [4]. The minor crystallographic diameter of cAMP, $2r \approx 5.2$ Å (Supplementary Figure 1, c), is such that $r/a \approx 0.3$ and the prediction is $p_u = 44.1\times10^{-3}$ μm^3/s, close to our experimental estimate ($47\pm15 \times10^{-3}$ μm^3/s). We refrained from extending these considerations to $InsP_3$ or LY, for which $r/a \approx 0.41$ and 0.49, respectively.

Computational details

The atomic model of the trans-membrane (TM) portion of HCx26wt connexon was constructed on the basis of the Cα model of mouse Cx32 reported by Fleishman et al. [1] (PDB entry code 1TXH). The sequence of HCx26wt was aligned to that of the Cx32 using T-COFFEE [5] and the coordinates of the matching Cα atoms were mapped. Additionally, charged residues next to the TM segments were added to consider electrostatic interactions that may potentially modify the conformation of the molecule. The final TM fragments in the HCx26wt subunits corresponded to: Ser19 to Glu42

(TM1), Arg75 to Ala96 (TM2), Leu132 to Val153 (TM3) and Glu187 to Leu209 (TM4). After Cα mapping from Cx32 to HCx26wt, all the atoms of the amino acids were added using their canonical conformation with the XLEAP module of the AMBER 8.0 software suite (http://amber.scripps.edu/). All chains were capped with N-methyl and acetyl groups, respectively, in order to avoid the spurious effects of terminal zwitterionic charges. This protocol yielded an atomic model with a large number of steric clashes and internal tensions that were relaxed using energy minimization (EM) and MD. Simulations were performed in the presence of implicit solvent with the Generalized Born approach [6] as implemented in AMBER 8.0 using the Amber94 force field [7]. A cutoff distance of 18 Å, a salt concentration of 0.15 M and a dielectric constant of 78 were adopted. The simulations used the Amber94 force field keeping the temperature at 100 K using Langevin dynamics with a collision frequency of 2 ps^{-1}. The *shake* algorithm was used to constraint all the chemical bonds. After full EM, the system underwent 50 ps MD with harmonic constraints applied on the Cα carbons. During this time interval, the positional constraints were decreased from 1 [kcal/mol-$Å^2$] to 0. Subsequently, 450 ps of free MD were performed. The stabilization of the root mean square deviations (RMSD) from the initial positions measured on the Cα atoms was taken as a criterion for structural relaxation of the model. RMSD reached stabilization after 250 ps, thereafter oscillating around a value of about 3 Å [8]. The diameter of the pore (17.5 Å) was measured on a structure averaged over the last 100 ps and fully minimized.

The molecular structures of $InsP_3$ and cAMP (in its *anti* conformation), were obtained from the PDB structures 1N4K [9] and 1Q5O [10], respectively. Since the structure of LY has not yet been solved by experimental techniques, structural models were constructed using WebLab ViewerPro (Accelerys). Molecular graphics and measures were performed with VMD [11].

References

1. Fleishman, S.J., Unger, V.M., Yeager, M. & Ben-Tal, N. A Calpha model for the transmembrane alpha helices of gap junction intercellular channels. *Mol Cell* **15**, 879-888 (2004).
2. Renkin, E.M. Filtration, diffusion, and molecular sieving through porous cellulose membranes. *J Gen Physiol* **38**, 225-243 (1954).

3. Unger, V.M., Kumar, N.M., Gilula, N.B. & Yeager, M. Three-dimensional structure of a recombinant gap junction membrane channel. *Science* **283**, 1176-1180 (1999).
4. Benedek, G., Villars, FMH in Biological Physics Series, Vol. 2, Statistical Physics, Second edition. (ed. E. Greenbaum) 91-261 (Springer-Verlag New York, Inc., New York; 2002).
5. Notredame, C., Higgins, D.G. & Heringa, J. T-Coffee: A novel method for fast and accurate multiple sequence alignment. *J Mol Biol* **302**, 205-217 (2000).
6. Tsui, V. & Case, D.A. Theory and applications of the generalized Born solvation model in macromolecular simulations. *Biopolymers* **56**, 275-291 (2000).
7. Cornell, W.D., P. Cieplak, C. I. Bayley, I. R. Gould, K. M. M. Jr., K. M. Ferguson, D. M. Spellmeyer, T. Fox, J. W. Caldwell, P. A. Kollman. A 2nd generation force-field for the simulation of proteins, nucleic acids, and organic-molecules. *J. Am. Chem. Soc.* **117**, 5179–5197 (1995).
8. Bicego, M. et al. Pathogenetic role of the deafness-related M34T mutation of Cx26. *Hum Mol Genet* **15**, 2569-2587 (2006).
9. Bosanac, I. et al. Structure of the inositol 1,4,5-trisphosphate receptor binding core in complex with its ligand. *Nature* **420**, 696-700 (2002).
10. Zagotta, W.N. et al. Structural basis for modulation and agonist specificity of HCN pacemaker channels. *Nature* **425**, 200-205 (2003).
11. Humphrey, W., Dalke, A. & Schulten, K. VMD: visual molecular dynamics. *J Mol Graph* **14**, 33-38, 27-38 (1996).

SUPPLEMENTARY FIGURE 1

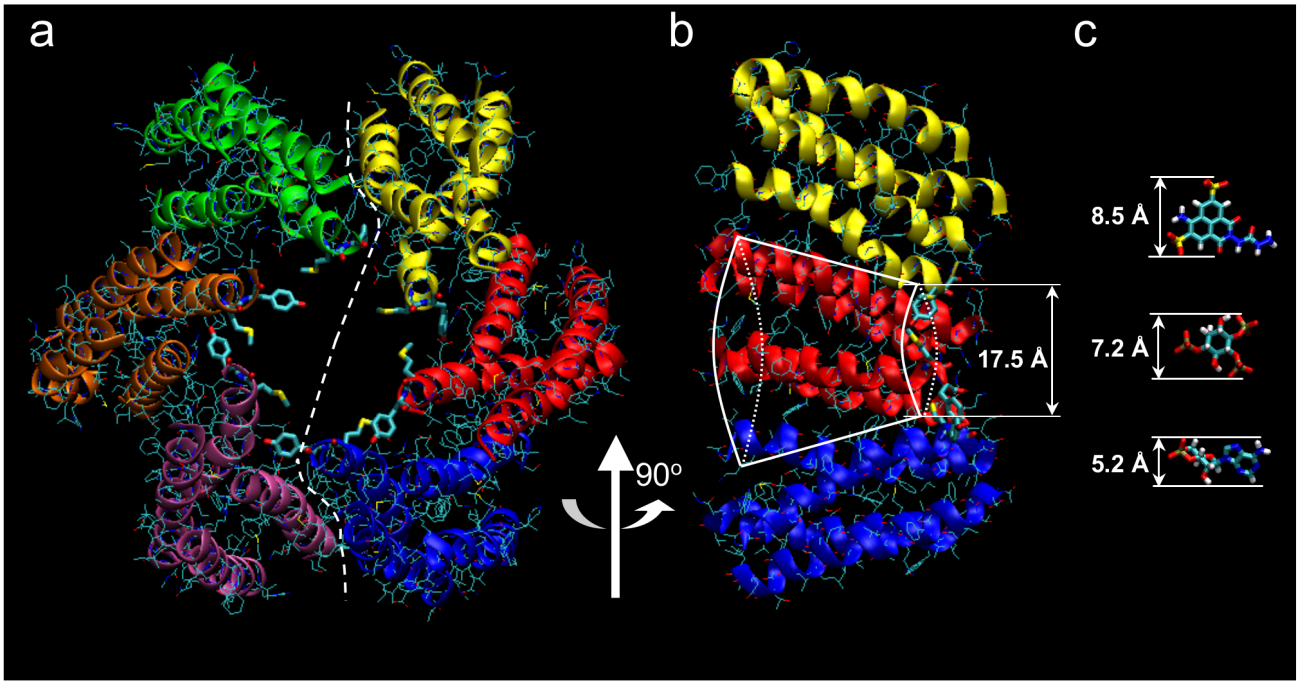

Supplementary Figure 1 Structural models of the HCx26wt connexon and permeant molecules. **(a**) Extracellular view of the atomistic model of the transmembrane part of the HCx26wt connexon. The differently colored ribbons indicate the diverse connexin proteins forming the connexon. Only heavy atoms are shown for visual clarity in line representation. Residues Met151 and Tyr152 that determine the maximum constriction belt are depicted with thick lines. The white dashed line indicates the dissection surface of the cross section of the model, shown in (**b**). (**c**) Molecular structures of LY, $InsP_3$ and cAMP (from top to bottom). The structures of the protein complex and permeating molecules are presented at the same scale to provide a comparative view. Minimal dimension are shown beside each molecule.